Correlating the Structure, Optical Spectra, and Electrodynamics of Single Silver Nanocubes

Jeffrey M. McMahon,[†,‡] **Yingmin Wang,**[§] **Leif J. Sherry,**[†] **Richard P. Van Duyne,**[†]
Laurence D. Marks,[§] **Stephen K. Gray,**[‡] **and George C. Schatz**[†,*]

*Department of Chemistry, Northwestern University, 2145 Sheridan Road, Evanston, Illinois 60208, Chemical
Sciences and Engineering Division, Argonne National Laboratory, Argonne, Illinois 60439, and Department of
Materials Science and Engineering, Northwestern University, 2220 North Campus Drive, Evanston, Illinois 60208*

The plasmonic properties of noble metal nanoparticles have potential uses in a wide variety of technologies, particularly sensing devices, based on their optical response. To better understand how nanoparticles can be incorporated in such devices, the detailed relationship between the optical response and structural properties of single nanoparticles is needed. Here we demonstrate that correlated localized surface plasmon resonance (LSPR) spectroscopy and high-resolution transmission electron microscopy (HRTEM) measurements can be used to obtain the optical response and detailed structural information for a single nanoparticle, using a silver (Ag) nanocube as the example. By carefully incorporating the HRTEM structural details into finite-difference time-domain (FDTD) electrodynamics calculations, excellent agreement with the LSPR measurements is obtained. The FDTD calculations show strong sensitivity between the nanocube optical response and the face-to-face width, corner and side rounding, and substrate of each cube, so careful determination of these parameters (1 nm resolution) is needed if theory and experiment are to match. In addition, the comparison of theory and experiment enables us to study the relative merits of the Johnson and Christy and Lynch and Hunter Ag dielectric data for describing perfect crystalline nanoparticles.

1. Introduction

Significant attention has been given to the study of the plasmonic properties of noble metal nanoparticles as a result of their potential uses as components in a diverse range of technologies, such as waveguides,[1–3] photonic circuits,[4,5] molecular rulers,[6] and chemical and biological sensors.[7–10] All of these applications are based on the localized surface plasmon resonance (LSPR) of each nanoparticle. LSPRs are excited when electromagnetic radiation interacts with a nanoparticle to create coherent oscillations (excitations) of the conduction electrons. This phenomenon has two key consequences: (1) selective photon absorption and scattering allows the optical properties of the nanoparticles to be monitored by conventional UV−Vis spectroscopy and far-field scattering techniques and (2) enhancement of the electromagnetic fields surrounding the nanoparticles leads to surface-enhanced spectroscopic techniques, such as surface enhanced Raman spectroscopy.[11] Previous studies show that the plasmon frequency is extremely sensitive to the nanoparticle composition,[12] size,[13] shape,[14–16] dielectric environment,[17–19] and proximity to other nanoparticles.[20–24] To better understand the design rules for practical plasmonic devices, the properties of single nanoparticles, including the relationship between particle morphology, substrate composition, plasmon spectral position(s), dielectric sensitivity, and sensing volume, need to be understood in greater detail. One way to study these relationships for a single nanoparticle is to make a correlated measurement, where for example, the optical response is measured with spectroscopy and structural information on

the same nanoparticle is obtained by microscopy.[25,26] One of the most detailed microscopy methods is high-resolution transmission electron microscopy (HRTEM), which can resolve subnanometer features and has ∼10 000 times higher magnification capabilities than optical microscopy. In addition, three-dimensional and internal crystallographic structural information can be obtained by using HRTEM via various techniques, such as electron energy loss spectroscopy and diffraction. Mie theory[27] can be used to analytically describe the relationship between the optical response, dielectric environment, and size of spherical nanoparticles. However, for more complex shapes analytical descriptions do not exist, and numerical methods, such as the finite-difference time-domain (FDTD) method,[28,29] must be used.

The goal of this work is to describe the relationship between the optical response, morphology, and dielectric environment of a single silver (Ag) cubic nanoparticle, a nanocube. A correlated LSPR-HRTEM measurement of the nanocube is presented, and using FDTD we carefully analyze the relationship between the nanocube optical response, face-to-face width, corner and side rounding, and substrate. We also assess the relative merits of the Johnson and Christy (JC)[30] and Lynch and Hunter (LH)[31] Ag dielectric data for describing perfect crystalline nanoparticles.

2. Experimental Methods

2.1. Materials. The substrate was a commercially available copper TEM grid with a 50-nm Formvar polymer and 2−3 nm amorphous carbon (C) layer (Ted Pella, Redding, CA). The grid was placed on an 18-mm No. 1 glass coverslip from Fischer Scientific (Pittsburgh, PA). Glassware preparations utilized H_2O_2, H_2SO_4, HCl, HNO_3, and NH_4OH from Fischer Scientific, and ultrapure H_2O (18.2 MΩ cm^{-1}) from a Millipore academic

* To whom correspondence should be addressed. E-mail: schatz@chem.northwestern.edu. Phone: 847-491-5657. Fax: 847-491-7713.
† Department of Chemistry, Northwestern University.
‡ Argonne National Laboratory.
§ Department of Materials Science and Engineering, Northwestern University.
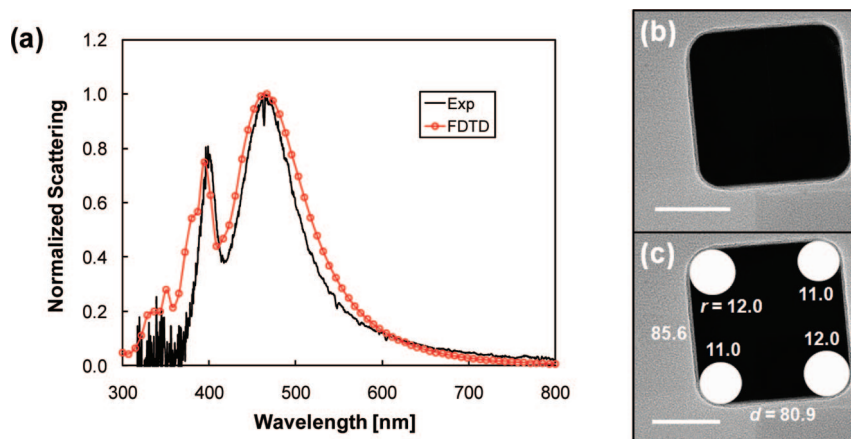
Figure 1. Correlated LSPR-HRTEM measurement of a single nanocube: (a) LSPR spectrum, (b) HRTEM image, and (c) HRTEM image with overlaid structural information (in nm). The inset white scale bars in panels b and c represent 40 nm. The FDTD calculated scattering cross section is also shown in panel a with open red circles.

system (Marlborough, MA). Trisodium citrate dihydrate and Ag nitrate (99.9999%) were purchased from Aldrich (Milwaukee, WI).

2.2. Synthesis of Nanocubes. Colloidal suspensions of Ag nanoparticles were synthesized by reducing Ag nitrate with sodium citrate, using an established scheme pioneered by Lee and Meisel.[32] Following this approach, 90 mg of Ag nitrate and 500 mL of ultrapure water were combined and brought to a boil in a cleaned ($3HCl:1HNO_3$) 1 L flask. Then, 10 mL of a 1% sodium citrate solution was added while stirring vigorously, and the resulting solution was boiled for 30 min. During this time, the solution underwent a color change sequence: first to light yellow followed by a change to opaque brown. The suspension was allowed to cool, and then transferred to a brown glass bottle for storage. Most of the nanoparticles in such a suspension are spherical in shape, with a diameter of ∼40 nm. However, many other geometries are also present, such as triangular prisms, rods, cubes, and hexagonal plates, which is easily verified by using electron microscopy.[17,33]

When ready to use, a 2−10 μL aliquot of nanoparticle solution was drop-coated onto the surface of a TEM grid. The substrate was then left to dry in air until the suspension droplet was no longer visible by eye. Samples were further dried in an N_2 environment for 1 h.

2.3. Optical Characterization. All single nanoparticle scattering spectra were obtained with either a Nikon Eclipse TE300 or Nikon Eclipse TE2000-U inverted optical microscope (Nikon, Japan) coupled to a SpectroPro 300i imaging spectrometer and a liquid nitrogen cooled Spec-10:400B CCD detector. These microscopes use a tungsten filament for illumination, which was focused on the surface of the sample by a Nikon 0.8−0.95 numerical aperture (NA) dark-field condenser. Single nanoparticles scatter this light into the collection optics. For our approach it was critical that the NA of the objective (collection optic) be smaller than the NA of the condenser so that none of the illumination light would be collected. A Nikon variable aperture (NA = 0.5−1.3) 100× oil immersion objective was chosen for this purpose. Figure 1 in the Supporting Information shows a schematic diagram of this apparatus.

To acquire a single nanoparticle scattering spectrum, the nanoparticle of interest was first imaged at the center of the spectrometer slit, which was narrowed to the diffraction limited spot size of the nanoparticle image. The grating was then rotated out of zero order into first order, and the dispersed light was imaged. WinSpec software (Princeton Instruments, Trenton, NJ)

was used to digitally select the region of the detector chip over which the nanoparticle's scattered light was located. A region of the same size was chosen where no nanoparticle scattering existed for background subtraction. The spectra were acquired and divided by the lamp spectrum.

To locate the same Ag nanoparticle for the TEM study, the asymmetric center of a TEM grid was used as a mark to define a coordinate for each section of the grid (Figure 2 in the Supporting Information). The grid was divided into four quadrants: (+,+), (+,−), (−,+), (−,−). Counting sections from the center grid mark gave the numeric value of the coordinate, while the sign of the number gave the quadrant. During the same time of the TEM study, a low-resolution optical image containing approximately all the particles in one specific section of the grid was recorded, as shown by Figure 3 in the Supporting Information. The TEM and optical images were used as pattern recognition maps to determine the relative locations of the nanoparticles.

2.4. Structural Characterization. Following the optical characterization, the same sample was transferred to a JEOL JEM-2100F Fast TEM (Tokyo, Japan), operating at an accelerating voltage of 200 kV, which was used to acquire all TEM data.

2.5. Computational Methods. FDTD calculations were carried out using standard techniques.[29] The computational domain was discretized using grid spacings of 1.0 nm, and terminated with convolutional perfectly matched layers (CPML). The dielectric functions of Ag and C were modeled using Drude plus 2 Lorentz pole functions (eq 1 in the Supporting Information) fit to empirically determined dielectric data[30,31,34] over wavelengths important to this study ($\lambda = 300-800$ nm). Formvar and glass were both modeled using a refractive index of $n = 1.5$. A Gaussian damped sinusoidal pulse with wavelength content over the range of interest was introduced into the computational domain using the total field−scattered field technique at normal incidence from the air side. Scattering cross sections were calculated by integrating the normal component of the Poynting vector over a boundary enclosing the particle using the scattered fields.

3. Results and Discussion

Colloidal Ag nanoparticles were synthesized and a correlated LSPR spectrum-HRTEM image of a single nanocube was obtained (Figure 1). From the HRTEM image (Figure 1c), the

Single Silver Nanocubes

J. Phys. Chem. C, Vol. 113, No. 7, 2009 **2733**

face-to-face widths are found to be 85.6(5) and 80.9(5) nm along both in-plane directions, with two of the corners rounded to 11.0(5) nm radii of curvature and the other two rounded to 12.0(5) nm. The structural information available from this image is limited by the TEM resolution and the top-down perspective. However, a cube height of 83(1) nm can be assumed by taking the average of the in-plane face-to-face widths, and the radii of curvature of the bottom edges and corners can be inferred from the corresponding top corners.

Two main peaks are observed in the LSPR spectrum, a narrow peak at 399 nm and a broad peak at 461 nm. The assignment of these peaks has been analyzed in detail previously,[17] where it was demonstrated that they are resonances associated with the tips of the cube where the electromagnetic fields are the most intense. Two peaks result from the two dielectric environments present, and have adiabatic correlations with the dipole and quadrupole resonances of the cube in a homogeneous environment. By analogy to the corresponding dipole and quadrupole resonances for spherical- or spheroid-shaped particles, the dipole resonance is expected to be broader than the latter due to important radiative damping effects.[15] Figure 1a shows that this analogy holds for the cube resonances, with the line width of the higher wavelength peak being 2.03 times that of the lower wavelength peak (experimental). Of course other effects can also contribute to the line widths, including charge transfer processes between the particle and its surrounding medium (so-called "chemical interface damping" effects[35]). However, in the present application the widths of the peaks seem to be well accounted for by electrodynamics calculations in which the particle and surrounding media are described using bulk dielectric constants (Figure 1a).

To determine the effects that the nanocube parameters and surrounding media have on the optical response, FDTD calculations were performed. The Ag nanocube was defined by its dielectric constant (JC or LH), face-to-face width (d), and radii of curvature of the corners and sides (r). Even though in the experiment each face-to-face width and radius of curvature of a corner or side is slightly different, they were assumed identical for the calculations. The nanocube was spaced by a distance h from a carbon (C) layer with thickness h_C. The C layer was placed on an infinite $n = 1.5$ substrate, and the surrounding medium was air ($n = 1.0$). Figure 2 shows a two-dimensional schematic diagram of the described system. Scattering cross sections for normal incident illumination were calculated for comparison with the experimental LSPR spectrum. Even though in the experiment the cube is illuminated at an angle and light is only collected for a range of angles around the forward direction (see Figure 1 in the Supporting Information), our past studies of these effects indicate that theory and experiment should have similar LSPR spectra. The scattering cross section of a nanocube with a face-to-face width of $d = 83$ nm and $r = 13$ nm of rounding, spaced $h = 2$ nm above an $h_C = 2$ nm thick C layer, and modeled with JC dielectric data is shown in Figure 1a, where excellent agreement with experiment is seen. The nanocube was positioned at $h = 2$ nm above the C layer to simulate the effect that the nanocube may not be resting directly on the substrate. This spacing could arise from physisorbed or weakly chemisorbed H_2O, CO_2, and hydrocarbons on the substrate, as well as citrate, O_2, and possibly hydroxyls on the nanocube surface. Depending on the thickness and dielectric constant of adsorbed molecules, the plasmon resonance positions and line widths will be affected, so other choices of h are
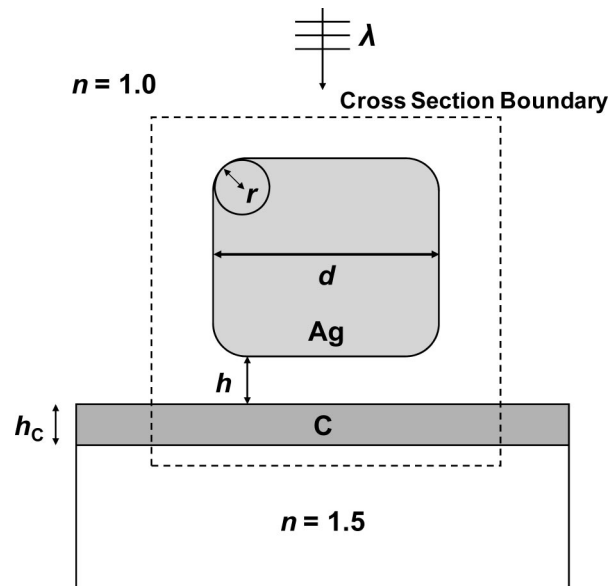

Figure 2. Two-dimensional schematic diagram of the nanocube system modeled with FDTD. The parameters in the figure are defined in the text.

considered below. Unfortunately we have no way to estimate the dielectric constant, so in the rest of this paper we have taken it to be 1.0.

Scattering cross sections were then calculated for nanocubes modeled by using the LH dielectric data with face-to-face widths of $d = 80$ and 90 nm and no rounding, and compared to experiment (Figure 3a). These parameters were chosen to elucidate only the effects due to the face-to-face widths, and are at the extremes of the actual parameters seen in the HRTEM image (Figure 1c). The $d = 80$ nm nanocube is seen to agree better with experiment, with the higher and lower wavelength peaks 21 and 10 nm closer to the experimental values, respectively. The difference in shifts is related to the smaller dielectric sensitivity of the lower wavelength (more quadrupolar) mode compared to the higher wavelength (more dipolar) mode, as noted previously for other particle shapes.[36] This effect arises from the shorter range of the near-field decay of the lower wavelength mode. However, even for the $d = 80$ nm nanocube, the calculated lower and higher wavelength peak positions are 35 and 44 nm red-shifted from the experimental values, respectively. This discrepancy arises from the choice of parameters other than the face-to-face width, which also have a large effect on the positions of both peaks and their relative amplitudes (see below).

Scattering cross sections were then calculated for a $d = 80$ nm nanocube with corners and sides rounded to various radii of curvature, and compared to experiment (Figure 3b). In addition, to increase the dielectric sensitivity we moved the nanocube to $h = 1$ nm above the C layer. The calculations show that the higher wavelength peak shifts by 41 nm as the radii increase from $r = 0$ to 12 nm, whereas the lower wavelength peak shifts by only 29.5 nm. These results are again related to the dielectric sensitivity of the quadrupolar mode versus the dipolar mode, and they highlight the importance of near-field contact area in determining the dielectric response of the nanocube, as has been found previously for other particle shapes.[37]

Additional insight concerning the effect of the C layer is provided by scattering cross sections calculated with the nanocube placed directly on the substrate, with and without C

**2734** *J. Phys. Chem. C, Vol. 113, No. 7, 2009*

McMahon et al.
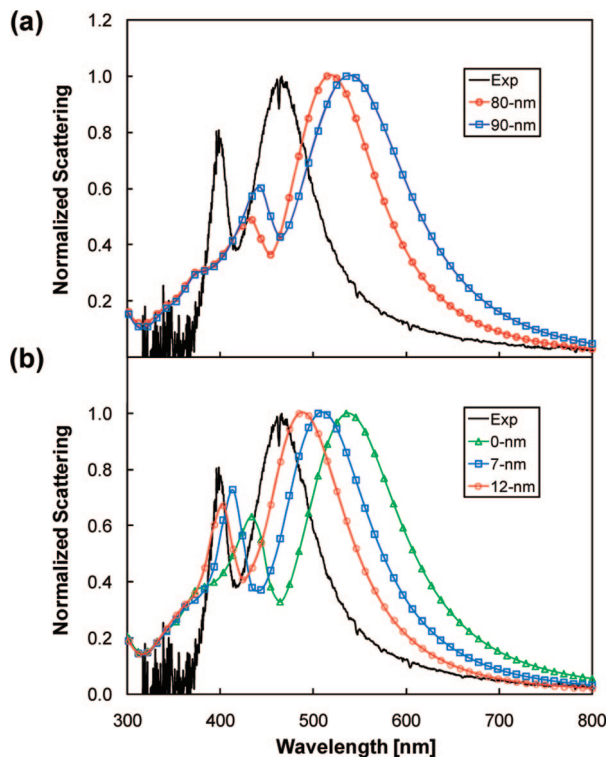
Figure 3. FDTD calculated scattering cross sections of a nanocube in response to (a) the variation in the face-to-face width with no corner rounding and placed $h = 2$ nm above the C layer and (b) the variation in the radii of curvature of the corners and sides of a $d = 80$ nm nanocube placed $h = 1$ nm above the C layer. In both cases, the nanocube is modeled by using the LH dielectric data and the C layer is $h_C = 2$ nm thick.
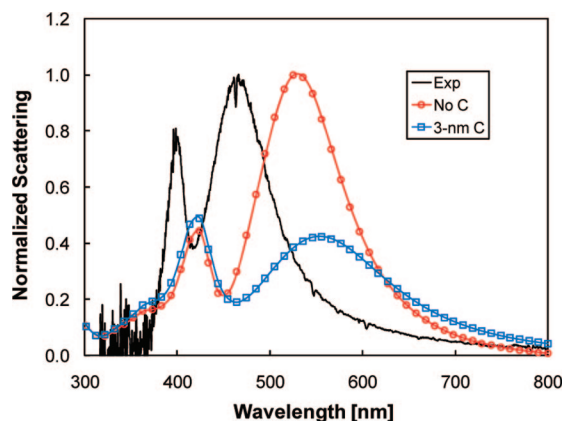
Figure 4. FDTD calculated effect of the C layer on a $d = 90$ nm nanocube. The nanocube is modeled with the LH dielectric data, has corners and sides rounded to $r = 7$ nm radii of curvature, and is placed directly on the C layer.

present (Figure 4). For these calculations, the contact area was made large by using a $d = 90$ nm nanocube with only $r = 7$ nm rounding, and the effect of C was heightened by making the layer $h_C = 3$ nm thick. The results show that the C has little effect on the lower wavelength peak, but red-shifts and significantly damps the higher wavelength peak. This is again related to the fact that the near-field decay of the lower wavelength mode is much shorter than the higher wavelength mode, and is therefore relatively unaffected by the substrate. These findings demonstrate the exquisite sensitivity of the plasmon resonance properties to substrate position and dielectric response, a result previously demonstrated by using gold
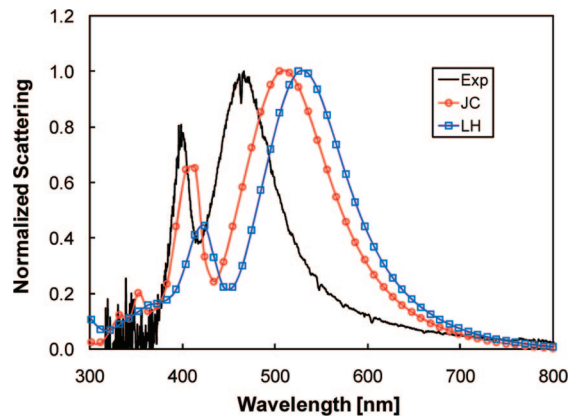
Figure 5. Comparison of JC to LH Ag dielectric data for modeling perfect crystalline nanoparticles, using a $d = 90$ nm nanocube as the example. The nanocube has corners and sides rounded to $r = 7$ nm radii of curvature and is placed directly on a $n = 1.5$ substrate with no C layer.

nanorings,[38] which gives us confidence that the optimal parameters that we have chosen to compare to experiment (Figure 1) are unique.

To assess the relative merits of the JC and LH Ag dielectric data when used to model perfect crystalline nanoparticles, scattering cross section of a $d = 90$ nm nanocube with $r = 7$ nm rounding were calculated and compared to experiment for both sets of data (Figure 5). For these calculations there was no C layer, and the nanocube was placed directly on the $n = 1.5$ substrate. It is seen that the JC data give results that agree much better with experiment, with the lower and higher wavelength peaks 10 and 21 nm closer to the experimental values, respectively. In addition, the JC dielectric data more accurately describe the width and relative amplitude of the lower wavelength peak. We should note that both the JC and LH dielectric data sets were inferred from thin films that are presumably polycrystalline or somewhat amorphous in character. It is therefore not a priori obvious why the JC dielectric data best describe our perfect crystalline nanoparticles. However, it has been found that for crystalline Ag nanowires the LH dielectric data provide a too lossy description, and effectively reducing the loss (more consistent with the JC dielectric data) improves agreement with experiment.[39] Similar conclusions were obtained in studies of Ag nanostrips made by using e-beam methods.[40]

4. Conclusions

Understanding the relationship between the optical response, structure, and dielectric environment of single nanoparticles is important to effectively design devices based on their plasmonic properties. Here we presented a detailed study of silver (Ag) nanocubes. A correlated LSPR spectrum-HRTEM image of a single nanocube was first obtained. FDTD calculations were then performed to study the relationship between the optical response, face-to-face width, radii of curvature of the corners and sides, and the substrate. It was found that all of these parameters have a large effect on the optical response, but if they are carefully incorporated into the FDTD calculations excellent agreement with experiment is obtained. In addition, it was found that the JC Ag dielectric data are more accurate for describing perfect crystalline nanoparticles compared to the LH dielectric data. These results demonstrate the importance of detailed structural and dielectric environment information in single nanoparticle studies for obtaining good agreement between experiment and theory.

Single Silver Nanocubes

J. Phys. Chem. C, Vol. 113, No. 7, 2009 **2735**

Supporting Information Available: Drude plus 2 Lorentz pole dielectric model for Ag and C, including a corresponding table of parameters and the function evaluation over the range $\lambda = 300-800$ nm; schematic diagram of apparatus used for measuring dark-field scattering; bright-field optical microscopy image showing the asymmetric center mark of a TEM grid; and an image showing the correlation of LSPR and TEM images. This material is available free of charge via the Internet at http://pubs.acs.org.

References and Notes

(1) Atwater, H. A. *Sci. Am.* **2007**, *296*, 56–63.
(2) Dionne, J. A.; Lezec, H. J.; Atwater, H. A. *Nano Lett.* **2006**, *6*, 1928–1932.
(3) Dionne, J. A.; Sweatlock, L. A.; Atwater, H. A.; Polman, A. *Phys. Rev. B* **2000673**, 035407/1–035407/9.
(4) Ozbay, E. *Science* **2006**, *311*, 189–193.
(5) Ebbesen, T. W.; Genet, C.; Bozhevolnyi, S. I. *Phys. Today* **2008**, *61*, 44–50.
(6) Reinhard, B. M.; Siu, M.; Agarwal, H.; Alivisatos, A. P.; Liphardt, J. *Nano Lett.* **2005**, *5*, 2246–2252.
(7) Haes, A. J.; Chang, L.; Klein, L. W.; Van Duyne, R. P. *J. Am. Chem. Soc.* **2005**, *127*, 2264–2271.
(8) Elghanian, R.; Storhoff, J. J.; Mucic, R. C.; Letsinger, R. L.; Mirkin, C. A. *Science* **1997**, *277*, 1078–1080.
(9) Anker, J. N.; Hall, W. P.; Lyandres, O.; Shah, N. C.; Zhao, J.; Van Duyne, R. P. *Nat. Mater.* **2008**, *7*, 442–453.
(10) McFarland, A. D.; Van Duyne, R. P. *Nano Lett.* **2003**, *3*, 1057–1062.
(11) Stiles, P.; Dieringer, J.; Shah, N. C.; Van Duyne, R. P. *Ann. Rev. Anal. Chem.* **2008**, *1*, 601–626.
(12) Link, S.; Wang, Z. L.; El-Sayed, M. A. *J. Phys. Chem. B* **1999**, *103*, 3529–3533.
(13) Haynes, C. L.; Van Duyne, R. P. *J. Phys. Chem. B* **2001**, *105*, 5599–5611.
(14) Jensen, T. R.; Malinsky, M. D.; Haynes, C. L.; Van Duyne, R. P. *J. Phys. Chem. B* **2000**, *104*, 10549–10556.
(15) Kelly, K. L.; Coronado, E.; Zhao, L. L.; Schatz, G. C. *J. Phys. Chem. B* **2003**, *107*, 668–677.
(16) Jin, R.; Cao, Y. C.; Hao, E.; Metraux, G. S.; Schatz, G. C.; Mirkin, C. A. *Nature* **2003**, *425*, 487–490.
(17) Sherry, L. J.; Chang, S.-H.; Schatz, G. C.; Van Duyne, R. P.; Wiley, B. J.; Xia, Y. *Nano Lett.* **2005**, *5*, 2034–2038.
(18) Xu, G.; Chen, Y.; Tazawa, M.; Jin, P. *J. Phys. Chem. B* **2006**, *110*, 2051–2056.
(19) Pinchuk, A.; Hilger, A.; Plessen, G. v.; Kreibig, U. *Nanotechnology* **2004**, *15*, 1890–1896.
(20) Malinsky, M. D.; Kelly, K. L.; Schatz, G. C.; Van Duyne, R. P. *J. Am. Chem. Soc.* **2001**, *123*, 1471–1482.
(21) Haynes, C. L.; McFarland, A. D.; Zhao, L.; Duyne, R. P. V.; Schatz, G. C.; Gunnarsson, L.; Prikulis, J.; Kasemo, B.; Kaell, M. *J. Phys. Chem. B* **2003**, *107*, 7337–7342.
(22) Zhao, L.; Kelly, K. L.; Schatz, G. C. *J. Phys. Chem. B* **2003**, *107*, 7343–7350.
(23) Huang, W.; Qian, W.; El-Sayed, M. A. *J. Phys. Chem. B* **2005**, *109*, 18881–18888.
(24) Gunnarsson, L.; Rindzevicius, T.; Prikulis, J.; Kasemo, B.; Kaell, M.; Zou, S.; Schatz, G. C. *J. Phys. Chem. B* **2005**, *109*, 1079–1087.
(25) Scherer, N. F.; Pelton, M.; Jin, R.; Jureller, J. E.; Liu, M.; Kim, H. Y.; Park, S.; Guyot-Sionnest, P. *Proc. SPIE* **2006**, *6323*, 632309/1–632309/6.
(26) Mock, J. J.; Barbic, M.; Smith, D. R.; Schultz, D. A.; Schultz, S. *J. Chem. Phys.* **2002**, *116*, 6755–6759.
(27) Mie, G. *Ann. Phys.* **1908**, *25*, 377–445.
(28) Yee, S. K. *IEEE Trans. Antennas Propag.* **1966**, *14*, 302–307.
(29) Taflove, A.; Hagness, S. C. *Computational Electrodynamics: The Finite-Difference Time-Domain Method*, 3rd. ed.; Artech House, Inc.: Norwood, MA, 2005.
(30) Johnson, P. B.; Christy, R. W. *Phys. Rev. B* **1972**, *6*, 4370–4379.
(31) Lynch, D. W.; Hunter, W. R. *Handbook of Optical Constants of Solids*; Academic Press: Orlando, FL, 1985.
(32) Lee, P. C.; Meisel, D. *J. Phys. Chem.* **1982**, *86*, 3391–3395.
(33) Wiley, B. J.; Sun, Y.; Xia, Y. *Acc. Chem. Res.* **2007**, *40*, 1067–1076.
(34) Arakawa, E. T.; Dolfini, S. M.; Ashley, J. C.; Williams, M. W. *Phys. Rev. B* **1985**, *31*, 8097–8101.
(35) Hovel, H.; Fritz, S.; Hilger, A.; Kreibig, U.; Vollmer, M. *Phys. Rev. B* **1993**, *48*, 18178–18188.
(36) Sherry, L. J.; Jin, R.; Mirkin, C. A.; Schatz, G. C.; Van Duyne, R. P. *Nano Lett.* **2006**, *6*, 2060–2065.
(37) Malinsky, M. D.; Kelly, K. L.; Schatz, G. C.; Van Duyne, R. P. *J. Phys. Chem. B* **2001**, *105*, 2343–2350.
(38) Larsson, E. M.; Alegret, J.; Käll, M.; Sutherland, D. S. *Nano Lett.* **2007**, *7*, 1256–1263.
(39) Laroche, T.; Vial, A.; Roussey, M. *Appl. Phys. Lett.* **2007**, *91*, 123101.
(40) Drachev, V. P.; Chettiar, U. K.; Kildishev, A. V.; Yuan, H.-K.; Cai, W.; Shalaev, V. M. *Opt. Express* **2008**, *16*, 1186–1195.

JP8098736